Available online at www.sciencedirect.com
ScienceDirect
Journal of Solid State Chemistry 181 (2008) 1116–1122
JOURNAL OF SOLID STATE CHEMISTRY
www.elsevier.com/locate/jssc

Reinvestigation of hybrid organic–inorganic materials based on molybdate and piperazininum cations: Influence of the synthesis conditions on the chemical composition and characterizations of the photochromic properties

Violaine Coué, Rémi Dessapt*, Martine Bujoli-Doeuff, Michel Evain, Stéphane Jobic

Institut des Matériaux Jean ROUXEL, UMR 6502 CNRS—Université de Nantes, 2 rue de la Houssinière, BP 32229, 44322 Nantes Cedex 3, France

Received 27 November 2007; received in revised form 11 February 2008; accepted 18 February 2008
Available online 25 February 2008

Abstract

The reactivity of the $[Mo_7O_{24}]^{6-}$ anion towards the structure directing-reagent piperazine (pipz) has been investigated and new synthetic routes to achieve the known $(H_2pipz)_3[Mo_8O_{27}]$ **1**, $(H_2pipz)[Mo_3O_{10}]\cdot H_2O$ **2**, and $(H_2pipz)[Mo_5O_{16}]$ **3** molybdenum(VI) containing compounds are proposed. The role of the pH on the stabilization of the different compounds and their interconversion pathways is discussed. Compounds **1** and **2** show photochromic behavior under UV excitation, related to the particular organization of the organic component around the mineral framework. Their optical properties are reported and commented.

Keywords: Organic–inorganic hybrid materials; Polyoxomolybdate; Piperazine; Photochromism

1. Introduction

Hybrid organic–inorganic materials based on isopolyoxomolybdate (Mo-POMs) and organoammonium cations may be viewed as potential photochromic materials [1]. Namely, these compounds exhibit white color in their ground state with an optical band gap assigned to an intramolecular oxygen to molybdenum charge transfer above 3 eV, and become colored under UV irradiation. In most cases, the coloration fades thermally or when samples are kept in the darkness for few hours. Since its discovery in the seventies [2], this particular optical behavior has triggered many investigations and a model based on the photogeneration of Mo(V) species, stabilized by the displacement of hydrogen atoms from the organoammonium cations to the Mo-POMs blocks has been proposed to account for the stability and color of the photogenerated state [3]. One recent major result rests on the tunability of the photochromic behavior by means of a proper choice of the organic and inorganic components [4]. Formally, the hue in the exited state, is mainly governed by the topology of the Mo-POM blocks, which dimensionality varies from isolated clusters (e.g. $[Mo_6O_{19}]^{2-}$, $[Mo_7O_{24}]^{6-}$, and $[Mo_8O_{26}]^{4-}$) to polymeric chains (e.g. $^1_\infty[Mo_3O_{10}]^{2-}$, $^1_\infty[Mo_8O_{27}]^{6-}$, and $^1_\infty[Mo_8O_{26}]^{4-}$) or layers (e.g. $^2_\infty[Mo_5O_{16}]^{2-}$ and $^2_\infty[Mo_7O_{22}]^{2-}$). The kinetics of the coloration/fading process strongly depends on factors such as the nature of the organic counter-cation (via its propensity to retrocede hydrogen atoms to the mineral part under UV–visible excitation) and the hydrogen bonding sub-network, i.e. the organic–inorganic interface. However, the design of new photochromic materials with specific photo-generated coloration is a hard challenge, principally because the stabilization of a specific Mo-POM fragment depends drastically upon numerous parameters such as pH, nature of the counter-cations, organic/molybdenum ratio, Mo VI precursors, temperature, solvent, and ionic strength of the mother solution. Specially, although it is often reported that organoammonium may act as structure directing-agent in the polymerization of the inorganic component in solution

*Corresponding author. Fax: +33 2 40 37 39 95.
E-mail address: remi.dessapt@cnrs-imn.fr (R. Dessapt).

0022-4596/$ - see front matter © 2008 Elsevier Inc. All rights reserved.
doi:10.1016/j.jssc.2008.02.010

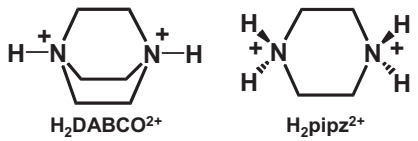

Scheme 1.

[5], the intimate dependence of the topology of a specific Mo-POM block upon the nature of the organic cation (i.e. its size, structure, charge, and number of potentially hydrogen bonding interactions) are nowadays unknown.

Recently, we reported that the reactivity of the discrete $[Mo_7O_{24}]^{6-}$ anion towards organoammonium dications such as H_2DABCO^{2+} (i.e. diprotonated diazabicyclo[2.2.2] octane) and H_2pipz^{2+} (i.e. diprotonated piperazine) (Scheme 1) led to a rich family of photochromic hybrid compounds containing a large variety of Mo-POM blocks [4]. Analyses of the $[Mo_7O_{24}]^{6-}$/DABCO system have highlighted the interconversion pathways between the different compounds as well as the role played by the pH, the DABCO/$[Mo_7O_{24}]^{6-}$ molecular ratio, and the temperature (ambient or hydrothermal conditions). Hereafter, we reported specific investigations on the $[Mo_7O_{24}]^{6-}$/pipz system in aqueous solution. To date, three hybrid organic–inorganic compounds built upon different Mo-POMs blocks and H_2pipz^{2+} cations have been prepared by three different authors, i.e. $(H_2pipz)_3[Mo_8O_{27}]$ **1** [6], $(H_2pipz)[Mo_3O_{10}]\cdot H_2O$ **2** [7], and $(H_2pipz)[Mo_5O_{16}]$ **3** [8]. This paper includes new synthetic routes of the three compounds with a clear evidence of the occurrence of $^1_\infty[Mo_3O_{10}]^{2-}$ chains in **2**. The influence of the pH on the stability of each molybdate block is clearly highlighted. Moreover, the optical properties of the materials are characterized and the photochromism of **1** and **2** is briefly discussed.

2. Experimental section

2.1. Materials and methods

Piperazine $N_2C_4H_{10}$ (pipz), $(NH_4)_6[Mo_7O_{24}]\cdot 4H_2O$ and MoO_3 were purchased from Aldrich. All reagents were used without further purification. All syntheses have been carried out using hydrothermal conditions (130 °C, 3 days) in 30 ml Teflon-lined autoclaves. The pH value, before and after hydrothermal treatment, is systematically mentioned.

2.2. Synthesis of $(H_2pipz)_3[Mo_8O_{27}]$ 1

$(NH_4)_6[Mo_7O_{24}]\cdot 4H_2O$ (1.236 g, 1 mmol) and pipz (0.344 g, 4 mmol) were dissolved in 15 ml of water. HCl 1 M was added dropwise in the mother solution until the pH ranged from 7 to 5. The mixture was stirred at room temperature for a few minutes and sealed in a 30 ml Teflon-lined autoclave. The slurry was filtered to isolate a white solid of **1**. The powder was washed with H_2O, EtOH, and Et_2O. The best yield (96% in Mo) is obtained for acidifying the mother solution at pH = 6 (final pH value = 6.5).

*Synthesis of **1** from **2***: **2** (0.277 g, 0.5 mmol) was slurred in 15 ml of water. After addition of an excess of pipz (0.108 g, 1.25 mmol), pH was adjusted with HCl 1 M until 6. The mixture was stirred at room temperature for a few minutes and sealed in a 30 ml Teflon-lined autoclave. The slurry was filtered to isolate a white solid of **1** (final pH value = 5.7). The powder was washed with H_2O, EtOH, and Et_2O (yield: 88% in Mo).

2.3. Synthesis of $(H_2pipz)[Mo_3O_{10}]\cdot H_2O$ 2

$(NH_4)_6[Mo_7O_{24}]\cdot 4H_2O$ (1.236 g, 1 mmol) and pipz (0.344 g, 4 mmol) were dissolved in 15 ml of water. HCl 1 M was added dropwise in the mother solution until the pH ranged from 4 to 2. The mixture was stirred at room temperature for a few minutes and sealed in a 30 ml Teflon-lined autoclave. The slurry was filtered to isolate a white solid of **2**. The powder was washed with H_2O, EtOH, and Et_2O. The best yield (96% in Mo) is obtained for acidifying the mother solution at pH = 3 (final pH value = 3.7). *Anal.* Calcd for $C_8H_{30}O_{11}N_2Mo_3$: C, 8.67; H, 2.54; N, 5.05; Mo, 51.96. Found: C, 8.91; H, 2.54; N, 5.20; Mo, 52.19. FT-IR (ν_{max}/cm^{-1}): H_2O, 1620 (w); H_2pipz^{2+} cations, 1463 (w), 1387 (w), 1320 (sh), 1230 (sh), 1082 (w), 1022 (sh), 1004 (sh), 978 (w) 610 (s), 592 (s); ν(Mo=O), 930 (m), 910 (s), 899 (s), 881 (s), 868 (s), ν(Mo–O–Mo), 640 (s), 479 (vs), 424 (vs).

*Synthesis of **2** from **1***: **1** (0.275 g, 0.19 mmol) was slurred in 15 ml of water and the pH was adjusted with HCl 1 M until 3. The mixture was stirred at room temperature for a few minutes and sealed in a 30 ml Teflon-lined autoclave. The slurry was filtered to isolate a white solid of **2** (final pH value = 4.1). The powder was washed with H_2O, EtOH, and Et_2O (yield: 92% in Mo).

*Synthesis of **2** from **3***: **3** (0.414 g, 0.5 mmol) was slurred in 15 ml of water. After addition of an excess of pipz (0.108 g, 1.25 mmol), the pH was adjusted with HCl 1 M until 3. The mixture was stirred at room temperature for a few minutes and sealed in a 30 ml Teflon-lined autoclave. The slurry was filtered to isolate a white solid of **2** (final pH value = 3.5). The powder was washed with H_2O, EtOH, and Et_2O (yield: 86% in Mo).

2.4. Synthesis of $(H_2pipz)[Mo_5O_{16}]$ 3

This material was prepared with $(NH_4)_6[Mo_7O_{24}]\cdot 4H_2O$ or MoO_3 as precursors. *Method 1:* $(NH_4)_6[Mo_7O_{24}]\cdot 4H_2O$ (1.236 g, 1 mmol) and pipz (0.861 g, 10 mmol) were dissolved in 15 ml of water. HCl 1 M was added dropwise in the mother solution until the pH ranged below 1. The mixture was stirred at room temperature for a few minutes and sealed in a 30 ml Teflon-lined autoclave. The slurry was filtered to isolate a white solid of **3**. The microcrystalline powder was washed with H_2O, EtOH, and Et_2O. The best yield (85% in Mo) is obtained for acidifying the

mother solution at pH = 1 (final pH value = 0.8). FT-IR (ν_{max}/cm^{-1}): H_2pipz^{2+} cations, 1469 (w), 1451 (w), 1442 (w), 1419 (w), 1377 (sh), 1317 (sh), 1213 (w), 1091 (w), 1057 (sh), 997 (sh), 974 (w); ν(Mo=O, Mo–O–Mo), 939 (s), 900 (s), 909 (s), 880 (s), 873 (s), 856 (vs), 752 (vs), 718 (s), 674 (vs), 594 (m), 545 (s), 518 (s), 459 (s), 423 (m).

Method 2: MoO_3 (0.720 g, 5 mmol) was slurred in 15 ml of water. After addition of pipz (0.086 g, 1 mmol), pH was adjusted with HCl 1 M until 1. The mixture was stirred at room temperature for a few minutes and sealed in a 30 ml Teflon-lined autoclave. The slurry was filtered to isolate a white solid of **3** (final pH value = 0.7). The powder was washed with H_2O, EtOH, and Et_2O (yield: 90% in Mo) [9].

*Synthesis of **3** from **2***: **2** (0.277 g, 0.5 mmol) was slurred in 15 ml of water and the pH was adjusted with HCl 1 M until 1. The mixture was stirred at room temperature for a few minutes and sealed in a 30 ml Teflon-lined autoclave. The slurry was filtered to isolate a white microcrystalline solid of **3** (final pH value = 1.2). The powder was washed with H_2O, EtOH, and Et_2O (yield: 94% in Mo).

2.5. Physical measurements

Elemental analyses of the solids were performed by the "Service d'Analyse du CNRS", in Vernaison (France). Powder X-ray patterns were collected at room temperature on a Siemens D5000 diffractometer without monochromator (CuK-L3,2), $\lambda = 1.540598$ and 1.544390 Å; Bragg–Brentano geometry; linear detector; 8–60° 2θ range). FT-IR spectra were recorded in the 4000–400 cm^{-1} range on a BRUKER Vertex equipped with an Attenuated Total Reflection (ATR) device from Specac Eurolabo and computer controlled using the OPUS software. Thermogravimetric (DSC-TGA) analyses were measured by flowing dry argon with a heating and cooling rate of 5 °C min^{-1} on a SETARAM TG-DSC 111 between 20 and 800 °C. Room temperature UV–vis diffuse reflectivity spectra were collected from a finely ground sample on a Cary 5G spectrometer (Varian). This instrument was equipped with a 60 mm diameter integrating sphere and computer controlled using the "Scan" software. Diffuse reflectivity was then measured from 250 to 830 nm (5–1.5 eV) with a 2 nm step using Halon powder (from Varian) as reference (100% reflectance). The photochromic properties were analyzed from powdered samples irradiated under a UV lamp ($\lambda_{exc} = 365$ nm (3.4 eV) or 254 nm (4.9 eV); $P = 12$ W, Fisher Bioblock labosi), for different durations until no significant change in the reflectivity spectra could be detected after one extra half-an-hour of irradiation. The absorption (α/S) data were calculated from the reflectivity using the Kubelka–Munk transformation: $\alpha/S = (1-R)^2/2R$, where R is the reflectivity at a given wavelength, α is the absorption coefficient, and S is the scattering coefficient. The latter was supposed to be particle size independent, as expected for particles with diameter larger than few micrometers. Practically, optical gaps are determined after a Kubelka–Munk transformation of the reflectivity spectrum as the intersection point between the energy axis and the line extrapolated from the linear portion of the absorption threshold.

3. Discussion

3.1. Hybrid organic–inorganic compounds based on Mo-POMs and H_2pipz^{2+} cations

Compounds **1**–**3** contain three different Mo-POM fragments displayed in Fig. 1, namely $^1_\infty[Mo_8O_{27}]^{6-}$ in **1**, $^1_\infty[Mo_3O_{10}]^{2-}$ in **2**, and $^2_\infty[Mo_5O_{16}]^{2-}$ in **3**. These blocks are connected with H_2pipz^{2+} cations via 3D array hydrogen bonding interactions.

$(H_2pipz)_3[Mo_8O_{27}]$ **1** was originally obtained from MoO_3 and piperazine [6]. Recently, we reinvestigated its structure and described it in terms of a mineral network composed of polymeric $^1_\infty[Mo_8O_{27}]^{6-}$ chains built upon γ-$[Mo_8O_{28}]$ subunits, connected each other by one common vertex, and maintained parallel by the H_2pipz^{2+} cations [4].

As $(H_2pipz)[Mo_3O_{10}]\cdot H_2O$ **2** precipitates in aqueous solution as white fibrillar crystal not suitable for X-ray diffraction investigation, its structure remains unfortunately unknown. However, its formulation has been confirmed by the self-consistent results of elemental analyses (vide infra), IR spectroscopy, and thermogravimetric measurements. The presence of the infinite $^1_\infty[Mo_3O_{10}]^{2-}$ chains has been evidenced by IR spectroscopy. Namely, the IR spectrum of **2**, displayed in Fig. 2, shows the absorption bands of H_2pipz^{2+} cations located between 1500 and 1000 cm^{-1}.

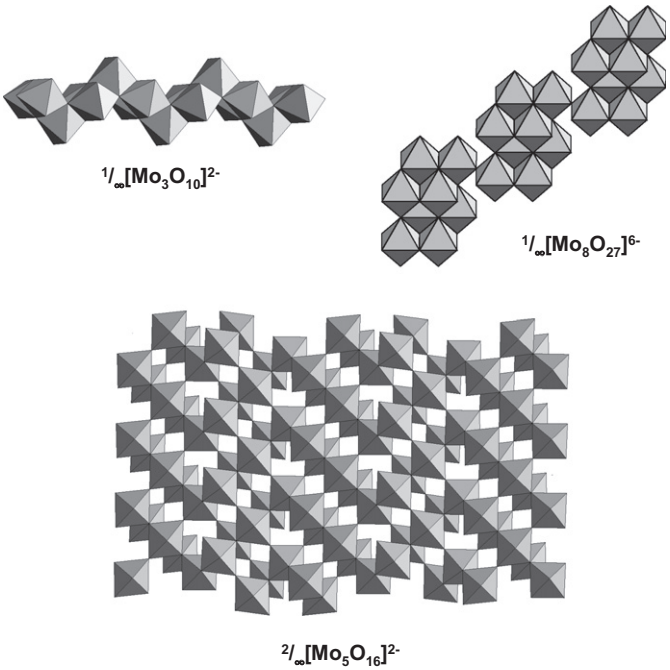

Fig. 1. Representation of the different $^1_\infty[Mo_8O_{27}]^{6-}$, $^1_\infty[Mo_3O_{10}]^{2-}$ and $^2_\infty[Mo_5O_{16}]^{2-}$ blocks in **1**, **2**, and **3**, respectively.

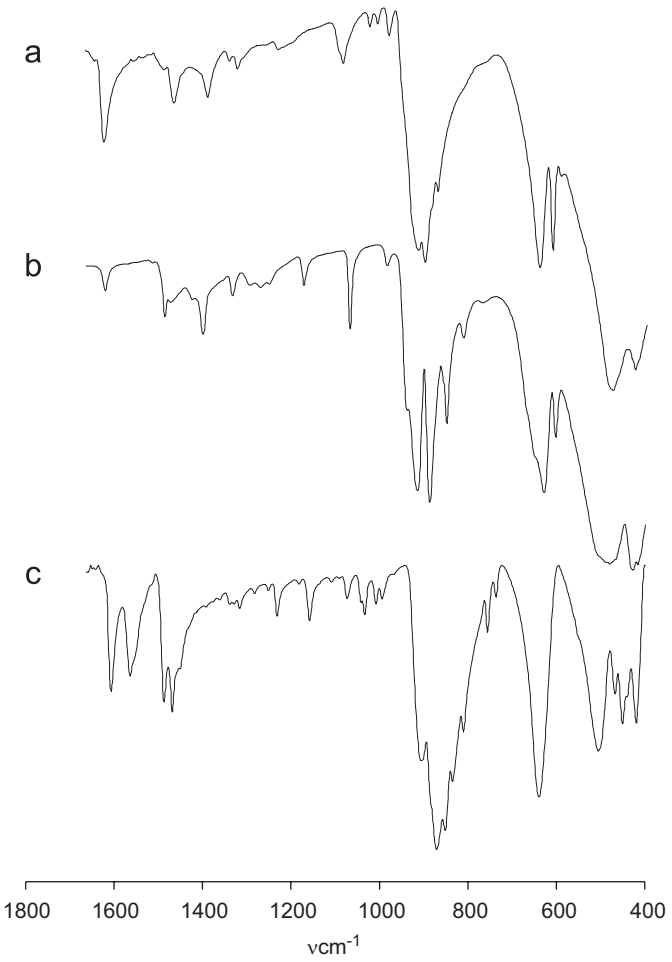

Fig. 2. Comparison between the IR spectra of: (a) **2**, (b) (H_2DABCO)$[Mo_3O_{10}]\cdot H_2O$, and (c) (1,6-H_2HDA)$[Mo_3O_{10}]$.

The existence of $^1_\infty[Mo_3O_{10}]^{2-}$ entities is evidenced by the absorption bands at 930, 910, 899, 881 and 868 cm^{-1}, related to $\nu Mo{=}O_t$ and $\nu Mo{-}O{-}Mo$, as observed in (H_2DABCO)$[Mo_3O_{10}]\cdot H_2O$ [4] and (1,6-H_2HDA)$[Mo_3O_{10}]$ [10]. Moreover, the TGA curve of **2** shows two main weight loss of 3.52% and 15.25%, appearing over the range 50–150 and 200–325 °C, respectively. The first one is due to the removal of the water molecule (theoretical weigh loss of 3.25%). The second one is attributed to the loss of one piperazine (15.5% of the total weight) and, consequently, to the decomposition of **2**.

(H_2pipz)$[Mo_5O_{16}]$ **3** is one of the rarest 2D hybrid material based upon molybdate and organoammonium cations. Its structure consists of the stacking of inorganic $^2_\infty[Mo_5O_{16}]^{2-}$ layers interspaced by H_2pipz^{2+} cations as showed in Fig. 3a. This inorganic layer has been described by Gatehouse et al. [11] in terms of infinite MoO_4 ribbons blocks with ReO_3-type structure, which are five octahedra wide, one octahedra deep and of infinite length connected by sharing octahedron edges, as displayed in Fig. 3b.

The purity of **1** and **3** samples was systematically checked by comparison of the experimental X-ray diffraction patterns with the simulated one issued from the single-crystal X-ray diffraction analysis of Harrison et al. [6] and Guillou et al [8].

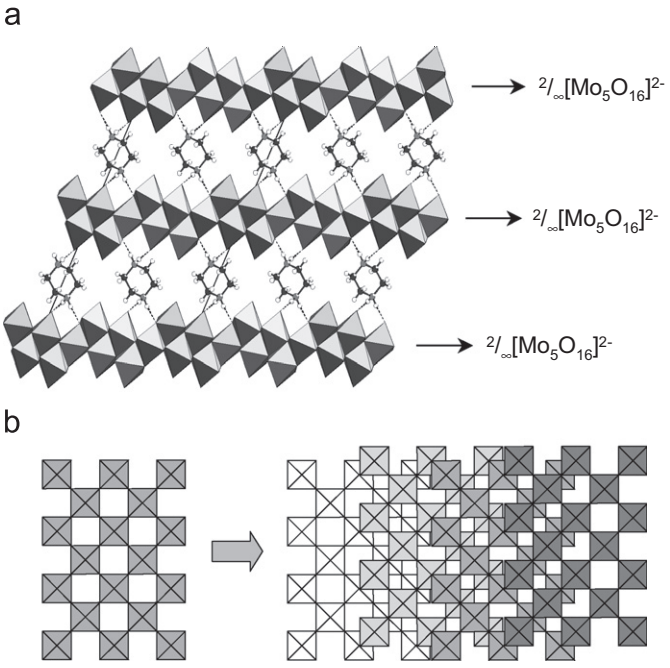

Fig. 3. (a) Representation of the arrangement of the $^2_\infty[Mo_5O_{16}]^{2-}$ blocks and the H_2pipz^{2+} cations in **3**. (b) Schematic stacking of the $[MoO_4]$ ribbons with ReO_3-type structure to form the $^2_\infty[Mo_5O_{16}]^{2-}$ layer in **3**.

3.2. Description of the $[Mo_7O_{24}]^{6-}$/piperazine system

The dependency of the topology of the Mo-POMs entities upon the pH is well known [12], but recent studies reported equally the influence of the content of organoammonium cations, when the pH is maintained constant [13]. However, similarly as we observed for the $[Mo_7O_{24}]^{6-}$/DABCO system, the pH is the main parameter to stabilize selectively the different Mo-POMs blocks in compounds **1**–**3**. The other parameters such as the temperature, which has been varied from 110 to 180 °C, the duration of the hydrothermal conditions or the piperazine/$[Mo_7O_{24}]^{6-}$ ratio (hereafter labeled N) ranging from 2 to 6, have no noticeable influence on the preparation of the materials from $[Mo_7O_{24}]^{6-}$, except for **3**, for which an excess of piperazine is required (vide infra).

As shown in Scheme 2, **1**, **2**, and **3** have been systematically isolated pure from $[Mo_7O_{24}]^{6-}$ and piperazine containing aqueous mother solution, for three distinct pH ranges, i.e. 7–5, 4–2 and below 1, respectively. The occurrence of $^1_\infty[Mo_8O_{27}]^{6-}$, $^1_\infty[Mo_3O_{10}]^{2-}$ and $^2_\infty[Mo_5O_{16}]^{2-}$ entities may be approached via acido-basic equilibria (Eqs. (1)–(3)), which allow to follow their prospective formation from acidified heptamolybdate aqueous solutions in specific pH range. As the pH decreases, the stability of the mineral species may increase in the sequence $^1_\infty[Mo_8O_{27}]^{6-} < {}^1_\infty[Mo_3O_{10}]^{2-} < {}^2_\infty[Mo_5O_{16}]^{2-}$.

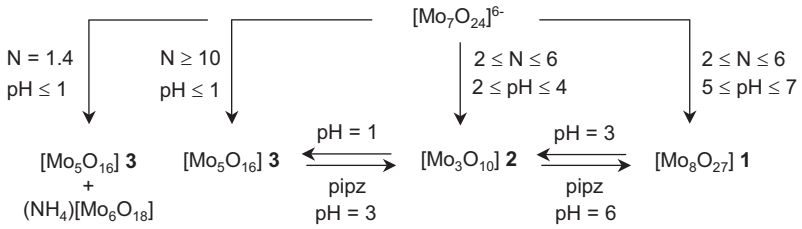

Scheme 2.

Table 1
Optical characteristics of compounds **1**–**3**

Compound	a	b	c	d	e	f
1	365 (3.4)	400 (3.1)	Yellowish white	Purple	517 (2.4)	260
2	254 (4.9)	331 (3.7)	White	Brown	477 (2.6)	250
3	365 (3.4) 254 (4.9)	376 (3.3)	White	White	–	–

a: UV excitation (nm (eV)); b: optical gap (nm (eV)) in stable state; c: color before irradiation; d: color after irradiation; e: center of the photo-induced absorption band in energy (nm (eV)); and f: duration after which no color evolution is observed under UV excitation (min).

The stabilization of the three Mo-POM blocks in **1**–**3** agrees well with this expected sequence.

$$8\ [Mo_7O_{24}]^{6-} + 6\ H^+ \rightarrow 7\ [Mo_8O_{27}]^{6-} + 3\ H_2O, \quad (1)$$

$$3\ [Mo_8O_{27}]^{6-} + 2\ H^+ \rightarrow 8\ [Mo_3O_{10}]^{2-} + H_2O, \quad (2)$$

$$5\ [Mo_3O_{10}]^{2-} + 4\ H^+ \rightarrow 3\ [Mo_5O_{16}]^{2-} + 2\ H_2O. \quad (3)$$

We highlight the quantitative interconversion process between the three compounds under hydrothermal conditions, by varying the H^+ or H_2pipz^{2+} contents, according to the theoretical acido-basic relations Eqs. (4) and (5). For instance, the expected conversion from a slurry of **1** in water to **2** occurs progressively by decreasing the pH, and is complete at pH = 3. In the same way, a slurry of **2** in aqueous solution acidified to pH = 1 triggers the appearance of **3**. The reverse conversion (**3**→**2** and **2**→**1**) occurs by increasing the content of piperazine and adjusting the pH value in the appropriate ranges.

$$3\ (H_2pipz)_3[Mo_8O_{27}]\ \mathbf{1} + 7\ H_2O + 2\ H^+ \rightarrow 8\ (H_2pipz)[Mo_3O_{10}]\cdot H_2O\ \mathbf{2} + H_2pipz^{2+}, \quad (4)$$

$$5\ (H_2pipz)[Mo_3O_{10}]\cdot H_2O\ \mathbf{2} + 4\ H^+ \rightarrow 3\ (H_2pipz)[Mo_5O_{16}]\ \mathbf{3} + 2\ H_2pipz^{2+} + 7\ H_2O. \quad (5)$$

The syntheses of **3** from $(NH_4)_6[Mo_7O_{24}]\cdot 4H_2O$ and piperazine needs to use a large excess of piperazine ($N \geqslant 10$). For this latter, the similar reaction realized with stoichiometric ratio ($N = 1.4$) systematically leads to a mixture of **3** and the hexagonal bronze phase $(NH_4)[Mo_6O_{18}]$ [14], which precipitates as a white-bluish microcrystalline solid. At 130 °C and for pH = 1, the H_2pipz^{2+} cations may act as reducting agents for a part of the Mo(VI) ions. Then, for $N = 1.4$, the NH_4^+ cations issued from the ammonium heptamolybdate precursor are the main counter-cation present in solution and they may be in competition with the H_2pipz^{2+} ones to direct the polymerization of the inorganic component. To avoid this competition, syntheses have been realized in a medium exempt of NH_4^+ cations, using MoO_3 and piperazine as starting materials. Then **3** has been successfully obtained pure with a high yield at pH = 1 with stoichiometric amount of piperazine (0.2 equivalent).

3.3. Optical properties

Under UV irradiation at 254 nm (4.9 eV) or 365 nm (3.4 eV), compounds **1**–**3** show different photochromic responses. Their optical properties are summed up in Table 1. Optical gaps, determined in their ground state, were calculated at 3.1, 3.7 and 3.3 eV for **1**, **2** and **3**, respectively, which agrees with the observed hues. Both **1** and **2** display a photochromic behavior under UV excitation, while **3** is not photochromic at all, even after excitation for periods as long as half a day.

The photochromic properties of **1** have been already reported in a previous paper [4]. This material undergoes purple coloration under UV excitation at 365 nm, due to the rising up of a broad absorption band located at 517 nm (2.4 eV). This specific photogenerated purple hue is characteristic in all photochromic $^1_\infty[Mo_8O_{27}]^{6-}$ chains containing organic–inorganic hybrid materials.

2 presents a light, reddish-brown coloration under UV excitation, which darkens with the irradiation duration. Under 254 nm excitation, color change is faster and much more intense than under 365 nm excitation. This stems from the higher value of the optical band gap in **2**, which implies a higher UV excitation energy to promote one electron from the valence band to the conduction one to generate the photochromic metastable state, according to Yamase's model [3]. The evolution of the optical properties of **2**, under illumination at 254 nm, is depicted in Fig. 4a.

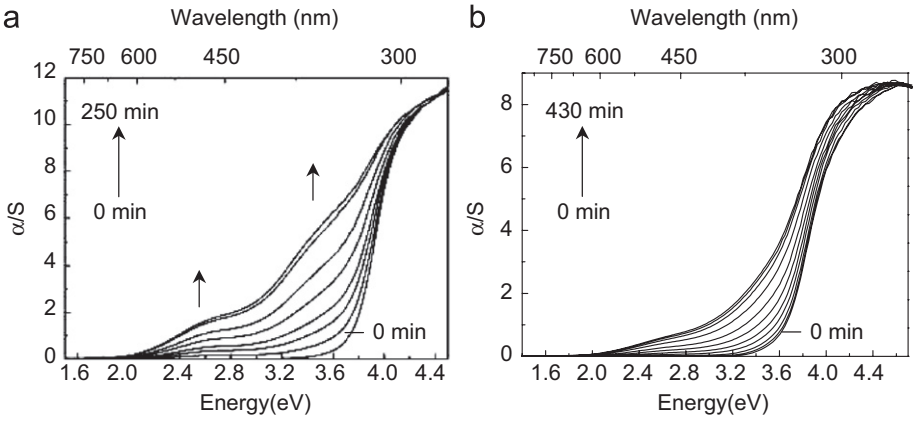

Fig. 4. Kubelka–Munk transformed reflectivity of **2** (a) and $(H_2DABCO)[Mo_3O_{10}]\cdot H_2O$ (b) vs. energy after irradiation at 254 nm for different durations (0, 10, 20, 40, 70, 110, 220, and 250 for **2** and 0, 20, 50, 90, 150, 210, 270, 330, 360, and 430 min for $(H_2DABCO)[Mo_3O_{10}]\cdot H_2O$).

Namely, a broad band located around 354 nm (3.5 eV) rises up with irradiation duration. Concomitantly, a second less intense broad band peaking at 477 nm (2.6 eV) rises up to a maximum reached after at least 250 min illumination. The absorption of **2** covers almost the whole visible spectrum and increases progressively in intensity from long wavelength to short wavelength, which explains the successive white, yellow brown, and reddish brown colors. Color change is detected by human eyes instantaneously after irradiation, and the photo-induced color does not evolve anymore after approximately 250 min. The evolution of the optical properties of **2** has been compared with the one of $(H_2DABCO)[Mo_3O_{10}]\cdot H_2O$ (Fig. 4b), which has been already reported [4]. This latter compound has appreciably the same absorption optical gap (3.6 eV) than **2** in the ground state, thanks to the presence of a similar $^1_\infty[Mo_3O_{10}]^{2-}$ block. The photochromic response of $(H_2DABCO)[Mo_3O_{10}]\cdot H_2O$ shows a broad band peaking at about 477 nm (2.6 eV), which rises up with irradiation duration with a progressive red shift of the absorption threshold with irradiation duration time. In regard with this new result, it appears that this red shift may be attributed to the grow of the second broad band located around 354 nm (3.5 eV), which is less pronounced compared to the one in **2**. The main difference between the photochromic responses of both compounds is that the coloration is faster in case of **2**, which agrees with the fact that the band at 477 nm (2.6 eV) reaches its maximum after 250 min for **2** and 430 min for $(H_2DABCO)[Mo_3O_{10}]\cdot H_2O$. We have already observed that the nature of the organic component may strongly influence the kinetics of the color change in such hybrid organic–inorganic materials [4]. In this case, the transfer of hydrogen atom from the H_2pipz^{2+} cation to the mineral framework seems to be more efficient than for the H_2DABCO^{2+} one. However, these results have to be considered carefully because of the lack of precise knowledge of the interactions at the interface of the organic and inorganic components in **2**.

The lack of coloration of **3** under UV excitation is surprising because the material exhibits all the factors deemed to favor photochromic properties. (i) Its quite low optical band gap (3.3 eV) may suggest an efficient electron transfer from the valence band to the conduction one, even at a 365 nm (3.4 eV) excitation. (ii) The nature of the organoammonium cations influences drastically the occurrence and the kinetics of the photochromism response in such hybrid materials. For example, the discrete $[Mo_7O_{24}]^{6-}$ cluster containing $(H_2DABCO)_3[Mo_7O_{24}]\cdot 4H_2O$ turns from white coloration to pink one under UV irradiation [4], while $(NH_4)_6[Mo_7O_{24}]\cdot 4H_2O$ is not photochromic at all. As both **1** and **2** are photochromic, H_2pipz^{2+} cations seems to be a well appropriated organoammonium cations for the design of photochromic hybrid materials. (iii) The photochromic process depends on the photo-activated transfer of one hydrogen atom from the organic component to the oxygen atom of the inorganic one via the hydrogen bonding interaction. For example, the lack of photochromic response in $(H_2DABCO)_2[Mo_8O_{26}]\cdot 4H_2O$ is attributed to the fact that the H_2DABCO^{2+} cations and the polymeric $^1_\infty[Mo_8O_{26}]^{4-}$ chains are indirectly linked through hydrogen bonding interactions with water molecules [4]. However, the H_2pipz^{2+} cations connect directly the inorganic $^2_\infty[Mo_5O_{16}]^{2-}$ layers in **3** via short hydrogen bonds, which are similar with these reported in **1** as shown in Supplementary Materials. All these results show that others parameters have to be considered to account for photochromism in such hybrid materials.

4. Conclusion

The rational design of solid materials from hydrothermal reactions hinges on the availability of a large panel of synthetic conditions to determine the key parameters which influence the appearance of mineral species. In the present case, the tricky question about the stabilization of $^1_\infty[Mo_3O_{10}]^{2-}$ and $^1_\infty[Mo_8O_{27}]^{6-}$ chains and $^2_\infty[Mo_5O_{16}]^{2-}$ layers in the hybrid $[Mo_7O_{24}]^{6-}$/pipz system was addressed via the investigation of the role of pH. The structural

preassembly of mineral entities in solution remains sketchy, but the overall features of the reactivity of the $[Mo_7O_{24}]^{6-}$ clusters in solution in hydrothermal conditions, as well as the interconversion pathways between **1**, **2**, and **3** have been identified. This augurs well for further studies on photochromism in hybrid organic–inorganic systems.

Appendix A. Supplementary materials

Supplementary data associated with this article can be found in the online version at doi:10.1016/j.jssc.2008.02.010.

References

[1] T. He, J. Yao, Prog. Mater. Sci. 51 (2006) 810–879.
[2] F. Arnaud-Neu, Ph.D. Thesis, University of Strasbourg, France, 1973.
[3] T. Yamase, Chem. Rev. 98 (1998) 307–325.
[4] V. Coué, R. Dessapt, M. Bujoli-Doeuff, M. Evain, S. Jobic, Inorg. Chem. 46 (2007) 2824–2835.
[5] P.J. Hagrman, D. Hagrman, J. Zubieta, Angew. Chem. Int. Ed. 38 (1999) 2638–2684.
[6] W.T.A. Harrison, L.L. Dussack, A.J. Jacobson, Acta Cryst. C 52 (1996) 1075–1077.
[7] The synthesis of **1** has been initially reported by Arnaud-Neu et al. (see Ref. [2]) from a more complex synthesis and without any data concerning the topology of the trimolybdate fragment.
[8] N. Guillou, G. Ferey, J. Solid State Chem. 147 (1999) 240–246.
[9] Initially, Guillou et al. reported the synthesis of **3** from MoO_3, $ZnCl_2$, piperazine and H_2O in the molar ratio 1: 1: 0.2: 80 at pH = 2 (180 °C, 24 h), but we show unambiguously that the use of $ZnCl_2$ are not necessary to stabilize this inorganic layer.
[10] D. Sun, H. Zhang, J. Zhang, G. Zheng, J. Yu, S. Gao, J. Solid State Chem. 180 (2007) 276–282.
[11] B.M. Gatehouse, B.K. Miskin, Acta Cryst. B 31 (1975) 1293–1299.
[12] J.J. Cruywagen, A.G. Draaijer, J.B.B. Heyns, E.A. Rohwer, Inorg. Chim. Acta 331 (2002) 322–329.
[13] J.H. Nelson, A.R. Johnston, A. Narducci Sarjeant, A.J. Norquist, Solid State Sci. 9 (2007) 472–484.
[14] C.-C. Jiang, G. Liu, Y.-G. Wei, W. Wang, S.-W. Zhang, Inorg. Chem. Commun. 2 (1999) 258–260.